HIGH SPECIFIC POWER MOTORS IN LN_2 AND LH_2

G. Brown*, R. Jansen†, J. Trudell*

* NASA Glenn Research Center, 21000 Brookpark Road, Cleveland, OH 44135, USA

† University of Toledo, 2801 W. Bancroft Street, Toledo, OH, 43606, USA

ABSTRACT

A switched reluctance motor has been operated in liquid nitrogen (LN_2) with a power density as high as that reported for any motor or generator. The high performance stems from the low resistivity of Cu at LN_2 temperature and from the geometry of the windings, the combination of which permits steady-state rms current density up to 7000 A/cm^2, about 10 times that possible in coils cooled by natural convection at room temperature. The Joule heating in the coils is conducted to the end turns for rejection to the LN_2 bath. Minimal heat rejection occurs in the motor slots, preserving that region for conductor. In the end turns, the conductor layers are spaced to form a heat-exchanger-like structure that permits nucleate boiling over a large surface area. Although tests were performed in LN_2 for convenience, this motor was designed as a prototype for use with liquid hydrogen (LH_2) as the coolant. End-cooled coils would perform even better in LH_2 because of further increases in copper electrical and thermal conductivities. Thermal analyses comparing LN_2 and LH_2 cooling are presented verifying that end-cooled coils in LH_2 could be either much longer or could operate at higher current density without thermal runaway than in LN_2.

KEYWORDS: high power density motor, cryogenic motor, high specific power motor

INTRODUCTION

It has been recognized for many decades that the windings of non-superconducting electromagnets benefit greatly from cryogenic cooling [1-5]. Electrical resistivities of pure metal windings can fall to a small fraction of room temperature values, reducing the power required to operate coils, and perhaps more importantly, reducing the amount of heat that must be removed and rejected to a cryocooler or a stored cryogen. High temperature superconductors have largely displaced pure metal conductors from consideration in high field solenoids and other DC applications. For motors, generators and other higher ramp-rate applications, however, pure metal conductors may still be competitive or even

preferred because of concerns about AC losses, structural robustness and electro-thermal stability in superconductors [6]. There are already niche applications for motors and generators submerged in cryogens in which the cooling is obtained easily and provides recognized benefits such as longer insulation life and relative compactness [7]. The highest specific power electric machines previously reported [8] are generators, one partially tested in LH_2 and one designed in detail for supercritical hydrogen.

The present investigation began under a program intended to evaluate electric drive of an aircraft fueled with LH_2 that would emit no CO_2. Non-electric aircraft fueled with LH_2 had been previously investigated and found plausible [9]. The primary obstacle to electric drive systems on aircraft (analogous to diesel-electric drive on locomotives and ships) has been the poor specific power of conventional electric machines. But cryogenic cooling may render electric drive competitive. Within some limits, LH_2 fuel could be used to cool propulsion motors and also generators and inverters in turbo-electric systems, before the fuel is burned [10]. In the present study, we consider motor coils that merely boil the cryogen, without utilizing the sensible heat of the vapor. Hydrogen-fueled aircraft are not presently under consideration, but using a small inventory of LH_2 as a coolant, re-condensed by a cryocooler, can still be considered for aircraft or other systems where high specific power is a major requirement.

In small electric motors operating at room temperature, the heat is often removed by conduction from one layer to the next to the surface of the coil for air cooling and/or to the poles on which the coils are wound, to be conducted to some other surface for ultimate rejection to air or another fluid. Layer-to-layer conduction is a poor mechanism of heat transfer in either potted or non-potted coils. At room temperature, conduction of heat along the wire to the end-turn region (where there can be more room for circulating a fluid to remove heat) is practical only for very short coils. But at cryogenic temperature, the heat production falls with the conductor's resistivity and thermal conductivity rises, making cooling at the end turns feasible. This allows coils of moderate length to operate in LN_2 at about ten times the current density possible in air at room temperature.

The temperature difference between the midplane and ends of current-carrying coils with heat rejection only at their ends is proportional to $J^2 L^2 \rho/\kappa$, for ρ/κ constant, where J is current density, L is coil length, ρ is electrical resistivity and κ is thermal conductivity. In LH_2 the product J*L can be increased because ρ/κ is smaller by perhaps a factor of 30 than at LN_2 temperature. LN_2, therefore, has been only a surrogate, used for convenience in the laboratory setting, for the intended cryogen LH_2. Fortuitously, the lamination stack length chosen for this test bed motor was short enough that the allowable current density in LN_2 generates specific power comparable to the best reported (assuming that we have obtained steady state operation rather than a transient overload condition).

It should be noted that while coil resistance and hence coil resistive losses fall dramatically with temperature, magnetic core losses do not. Reduction of core losses can only be addressed by geometric and material changes of the core. We do not consider the core here.

We first present some experimental measurements on the current carrying capacity of free-standing coils in LN_2, followed by measurements of motor power produced by using the coils. Then we present an analysis of the heat transfer for end-cooled coils, comparing the LN_2 coil test results with the analysis, followed by an examination of the degree of improvement possible with LH_2 over LN_2.

COIL PERFORMANCE IN LN_2

Some current capacity measurements on copper coils with partially spaced end turns were previously reported in [10]. The present measurements are on coils in which both

sides of every layer are exposed to LN_2 in the end turn region. In addition to steady state measurements, the transient approach to steady state was measured to guide our motor testing, which has a limited supply of LN_2. The time constants for approach to thermal steady state will get shorter with lower temperature because of the considerable decrease in heat capacity, as well as a moderate increase in thermal conductivity. The thermal time constant at room temperature for tightly wound coils with only natural convection to air for heat removal can be 5 to 10 minutes or more, mainly because of poor heat transfer between coil layers and from the coil surfaces. The coil surfaces can be many tens to a hundred degrees or more hotter than the ambient air. For end-cooled coils in LN_2, as long as a transition from nucleate to film boiling is avoided, the superheat (surface temperature minus bulk liquid temperature) of the cooled surfaces is never more than 12 K (see the appendix). The need for layer-to-layer heat transfer is eliminated completely, though the temperature rise of the coil midplane needed to transfer the heat by conduction to the end turns poses a new performance limit.

FIGURE 1(a) shows a photograph of one of the coils tested and FIGURE 1(b) shows the steady state resistance of the coil as a function of current (DC) in LN_2. Note that the coil can carry over 70 A DC, which would translate to 100 A current in the motor at a 50 percent duty cycle (which we seek in order to achieve maximum torque and power). At 72.9 A the resistance increases indefinitely.

The approach of coil resistance to a steady state for four values of suddenly applied current is shown in FIGURE 2 along with a runaway condition at 72.9 A. Temperature is not measured; rather the resistance is used as an indication of temperature. One sees that the approach to steady state is faster at 39.4 A than at 71.1 A. At the higher currents the resistance rises appreciably before steady state is reached. In fact it would be expected that the time to approach the final state becomes infinitely long for the highest current that actually has a steady state rather than an unstable runaway. At 39.4 A, the change in resistance reaches 90 percent of its ultimate value in about 4 seconds; at 71.1A it requires four times as long.

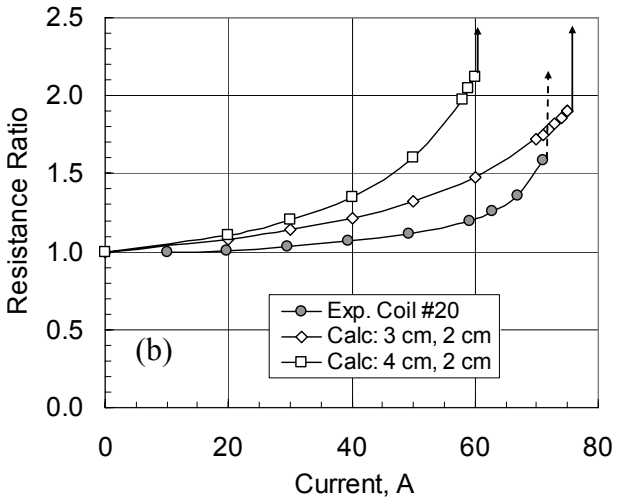

FIGURE 1. (a) Photograph of 6-layer coil. (b) Steady-state resistance, normalized to un-powered resistance, as a function of direct current for that coil, measured and calculated. Arrows indicate thermal runaway. Calculated results are discussed in a later section.

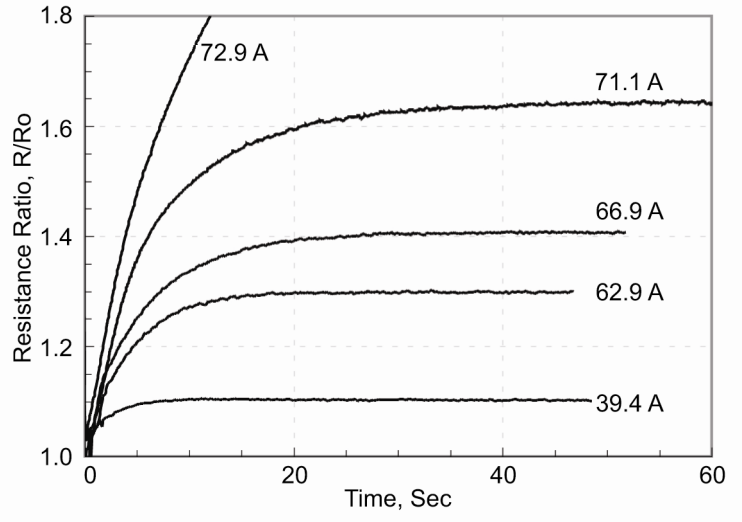

FIGURE 2. Response of resistance to step function of current. At 72.9 A, a steady state is never reached.

MOTOR PERFORMANCE IN LN_2

The switched reluctance motor (SRM) is recognized as a robust high performance electric machine which has been studied for aircraft applications. One of the highest specific powered SRMs reported, a prototype for an aircraft electric fuel pump, is described in [11].

The present motor was described at an earlier state of development in [14]. It is a "12/8" machine (12 stator poles and 8 rotor poles) with a 10 cm (4 in.) diameter rotor and a 5.08 cm (2 in.) axial stack of commercial 6 mil Fe49-Co49 "high strength" laminations on both rotor and stator. The motor has a vertical axis to facilitate submersion in LN_2, even though a horizontal axis is envisioned in actual application, necessitating eventual design changes for fluid handling. The stator FIGURE 3(a), rotor FIGURE 3(b), and lower bearing are all submerged in LN_2; the upper shaft bearing is at room temperature. The motor pole laminations operate far into magnetic saturation (though the backiron does not) due to the 6,000 to 10,000 A-turns of excitation on each pole and a 0.5 mm (20 mil) radial magnetic gap. Various coil configurations have been matched to the available power source, all employing varying numbers of paralleled #18 wire coils. Commercial 6-switch inverters were adapted to operate as asymmetrical bridges that provided up to 100 A current into each parallel section. The currents were controlled by a mixed digital/analog hysteresis controller that produced as close to a square-wave as the available voltage, inductance, back emf and switching rate would allow. Our goal being high specific power, we used a 50 percent duty cycle in preference to the 33 percent that would give minimum torque ripple at moderate speed. Therefore our maximum currents of 100 A amplitude would correspond to 71 A rms or DC if square waves were actually achieved. The typical wave form however had a lower rms value.

Torque was measured with an eddy current dynamometer. To save on power electronics, only two coils of the twelve were energized for the high power tests. Drag torque was measured in un-powered spin-down tests. Test times at high power were typically limited to 5 seconds (shorter than the time shown above to be required to reach steady state) because of the limited inventory of LN_2 in the experimental dewar. However, as shown in FIGURE 2, a single isolated coil immersed in LN_2 can sustain over 70 A rms. We must yet show that, in the confines of the motor and for runs lasting a half minute or more, fresh liquid is supplied to the coils and gas bubbles are removed rapidly enough

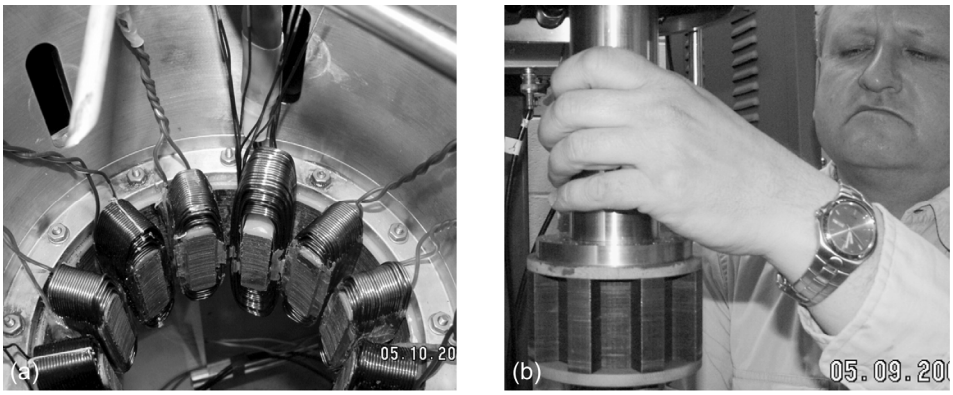

FIGURE 3. (a) Stator of 12/8 switched reluctance motor with various developmental coils. (b) Rotor.

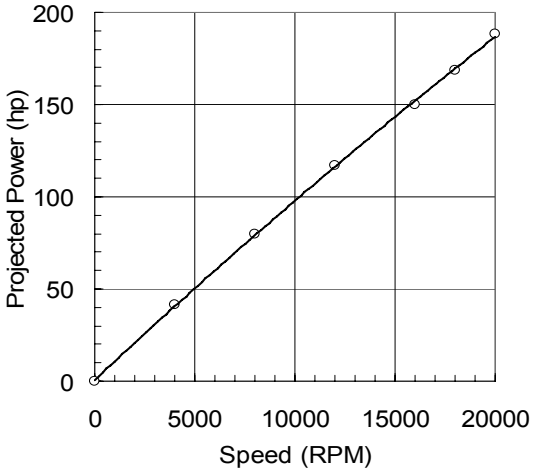

FIGURE 4. Projected 12-coil power based on measured shaft output power with two coils energized, corrected for drag, which was measured in un-powered spin-down tests.

to prevent vapor blanketing of the coils. The phases of switched reluctance motors are well known to be independent, as long as the back iron does not saturate. The back iron of this particular motor does not reach saturation even at our highest currents; hence we can take the measured performance from two energized poles and project it to twelve, making appropriate allowance for drag. The power projected in this way is plotted as a function of speed in FIGURE 4.

If subsequent testing shows a thermal steady-state has been achieved, the specific power of this SRM would equal or exceed the specific power of any other tested electric machines known to us. Our highest projected power to date, 141 kW (189 hp) in the 8.1 kg-EM (17.8 lb) motor, corresponds to a specific power of 17.4 kW/kg-EM (10.6 hp/lb-EM), about twice that of the room temperature SRM in [11]. (EM denotes electromagnetic mass—the mass of coils and laminations.) Assuming a 60 percent increase in mass to 13.0 kg for the balance of the motor, the specific power would be 10.8 kW/kg (6.6 hp/lb), similar to the 10 kW/kg capability reported in [12] for a non-superconducting 1 MW exciter operating near LH_2 temperature.

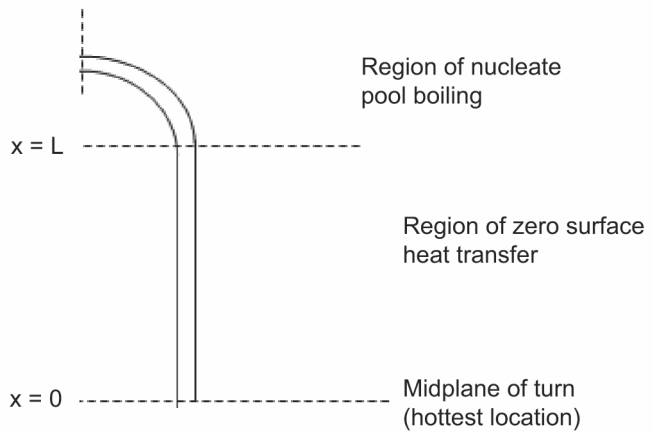

FIGURE 5. One quarter of one turn of a multi-turn, multi-layer coil. The lengths of the cooled quarter-circle are assumed to be 1 cm for the calculations presented in FIGURE 6 and 2 cm for the results in FIGURE 1.

COMPARATIVE ANALYSIS OF END-COOLED COIL HEAT TRANSFER IN LN_2 AND LH_2

We used a relatively simple and approximate way to predict the current capacity of end-cooled motor coils. The data above, taken in LN_2, roughly validate the analysis and give confidence that the analysis can predict results for LH_2, for which we do not yet have experimental data. Highly quantitative validation of the LN_2 analysis is not possible because the experimental data is for multi-turn, multi-layer coils, which can reveal only the average behavior for turns with varying lengths and locations. Furthermore the LH_2 predictions will be only approximate because variations in composition and strain history affect resistivity so strongly.

We analyze a single turn which is thermally independent of its neighbors; one quarter of such a turn is illustrated in FIGURE 5. Joule heating occurs everywhere in the turn in proportion to the local temperature-dependent resistivity. Heat transfer from the wire occurs only from the surface of the curved end-turn region, immersed in the cryogen. The hottest point will be at the coil midplane and the coolest point at the center of the end-turn. The point at which the cooled and un-cooled sections join will have the highest superheat of the cooled region and would be the inception point for film boiling, should the surface heat flux be too high there. In the adiabatic straight section, the temperature T in a thermal steady state, as a function of distance x from the midplane, obeys

$$\kappa \, d^2T/dx^2 = -J^2\rho(T) \tag{1}$$

where κ and ρ are the thermal conductivity and electrical resistivity respectively of copper, J is current density in the wire and T is absolute temperature. Within each temperature range of our interest, the variation of thermal conductivity of copper is not nearly as important as the variation of resistivity, and we treat the former as a constant in each temperature range. If resistivity were also constant with temperature, the solution of equation (1) would be

$$T(x) - T(L) = J^2 \, (L^2 - x^2) \, \rho/(2 \, \kappa \,) \tag{2}$$

where x is measured from the coil mid-plane, L is the half-length of the straight, uncooled section and $T(L)$ is the temperature at $x = L$, the junction of the straight and curved portions

of the turn. The midplane temperature $T(0)$ would then exceed the temperature $T(L)$ at $x = L$ by

$$T(0) - T(L) = J^2 L^2 \rho/(2 \kappa). \quad (3)$$

Both J and L appear quadratically, J because heating is proportional to J^2, and L because of the distributed nature of the electrical heating. Thus reductions of the quotient (ρ/κ) allow increases in the product of J and L. Equation (3) gives only a lower bound on the midplane temperature; the actual value will be higher because of the increase of resistivity as the coil heats and because of the superheat of the wire surface in the immersed region, required to reject the heat. A linear approximation for resistivity is adequate near LN_2 temperature. But near LH_2 temperature we use a quadratic approximation to the resistivity, which makes equation (1) non-linear and precludes an analytical solution. The electrical resistivity and thermal resistivity of copper and other pure metals vary so much near LH_2 temperature that only approximate treatment is warranted.

The models used for the copper transport properties and for the nucleate boiling cooling of the end section are given in the appendix. To take into account the heat flux from the surface of the wire in the cooled end turn, a term proportional to the nucleate boiling heat flux as a function of the temperature difference between the local wire surface and the bulk liquid temperature must be added to the right hand side of equation (1). For solution, however, we recast the problem into integral form and solve iteratively only for the final steady state temperature distribution and resistance.

Although the experimental work has been confined to coil measurements and motor testing in LN_2, the advantages of cryogenic operation will be more pronounced with LH_2. An examination of Table 1 shows several favorable changes in copper and fluid properties in going from LN_2 to LH_2 and only one or two adverse changes. The most marked changes are in Cu resistivity and heat capacity, which, at LH_2 temperature, are respectively about 1/14th and 1/22nd of their LN_2 values. Heat capacity affects the rate of approach to thermal steady state but not the final temperature distributions. The thermal conductivity of commercial copper wire roughly doubles from LN_2 temperature to LH_2 temperature. The

TABLE 1. Copper and fluid properties at room, LN_2 and LH_2 temperatures

Property	Unit	(300K)	LN_2 (77K)	LH_2 (20.4K)
Cu resistivity*	μΩ-cm	1.7	0.23	0.017*
Cu thermal conductivity*	W/cm-K	4	5	10*
Cu heat capacity (Θ_D = 396K)	J/g-K	0.38	0.20	0.009
Cu thermal diffusivity*	cm^2/sec	1.2	2.8	124*
critical nucleate pool boiling heat flux	W/cm^2	--	20	10
superheat at critical heat flux	K	--	12	3.3
heat of vaporization per mass	J/g	--	199	446
heat of vaporization per liquid volume	J/liq-cm^3	--	161	32
heat of vaporization per gas volume	J/gas-cm^3	--	0.91	0.58
gas density at normal b.p.	g/cm^3	--	0.0046	0.0013
liquid density	g/cm^3	--	0.81	0.071
gas to liquid molar volume ratio at b.p.	--	--	176	55

*N.B. Cu transport properties are approximate. A round number of 100 is used for the ratio of Cu resistivity at room temperature to resistivity at LH_2 temperature because the latter resistivity depends so strongly on purity, work hardening and even magnetic field.

volume of boil-off gas is reduced because of the resistivity drop, which more than offsets the unfavorable drop in heat of vaporization per unit volume of boil-off gas. The fluid viscosity is lower, facilitating coolant flow.

For examples of the improvement obtained in end-cooled coil performance, we show some calculated results, most that are near the allowable limits of current and length, first for LN_2 then for LH_2. FIGURE 6(a) presents a number of final steady temperature distributions in LN_2 for a quarter turn like that in FIGURE 5 and FIGURE 6(b) presents LH_2 results. Consider the calculated result in (a) for L = 3 cm and 4 cm, the curved quarter-circle length of 1 cm and a current of 60 A rms. These values of L are close to representing the experimentally measured coils. For L = 4 cm the junction between the cooled and un-cooled sections, marked by an open circle at x = 4 cm, operates at 88.7 K. This is very close to the 89 K value (corresponding to 12° of superheat above the LN_2 normal boiling point of 77 K) at which a transition to film boiling would occur, resulting in a severe drop in heat transfer (to about 1 or 2 W/cm^2 instead of 20 W/cm^2) and an ensuing thermal runaway. (See the nucleate boiling data in the appendix and film boiling data in [15] and [16].) The midplane of the coil reaches a steady state of 140 K, nearly twice the absolute temperature of the fluid. For a slightly higher current there is no stable steady state solution; rather the temperature and resistance increase indefinitely. Depending on the parameters this thermal runaway may originate from inadequate conduction to the end region of the coil or from a transition to film boiling which causes inadequate surface heat flux from the end turn to the liquid. Both of these causes are close to occurring for the 4 cm, 60 A case. The other curves in FIGURE 6(a) show that if the un-cooled half-length is reduced to 3 cm, the point of greatest superheat at x = 3 cm is only at 85 K and the midplane at 103 K for 60 A. At 70 A these temperatures rise to 88 K and 118 K. The calculated resistances for the three cases at steady state are 2.3, 1.6, and 1.9 times their un-powered values, respectively. Only resistances were experimentally measured; temperatures were not. Cases for L = 3 cm and 4 cm, with a curved quarter-circle length of 2 cm, more closely match our coil geometry and are compared to the experimental results in FIGURE 1(b), showing rough agreement on the range of current where thermal runaway occurs and thereby providing design guidance. But more detailed modeling of the heat transfer from layer to layer, in addition to better assessment of where along the wire the nucleate boiling cooling begins, would be required for close quantitative agreement.

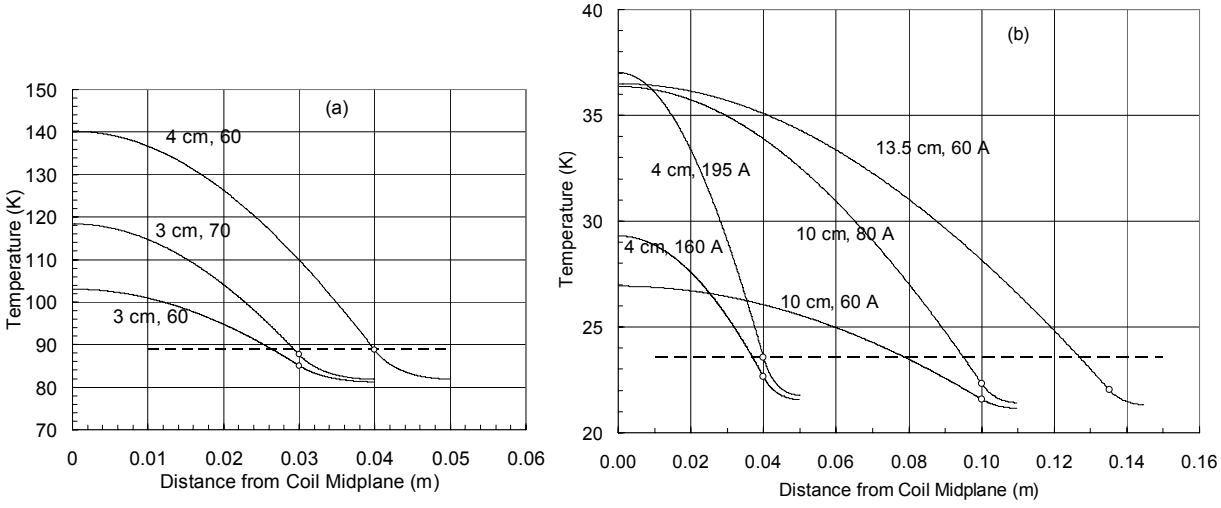

FIGURE 6. Calculated temperature distributions in a quarter turn for various combinations of current and un-cooled half-length L. The wetted length in the quarter turn is 1 cm for these calculations. (a) LN_2 results. (b) LH_2 results.

It is seen from the analysis that in LN_2 the un-cooled half-length of the longest turns in a motor coil operating at 60 A rms can be no more than about 4 cm (with cooled section of 1 cm length) to avoid thermal runaway. This means that the lamination stack height must be less than 8 cm (3.1 in) or less for end-turn cooling to be successful at that current.

The calculated results for LH_2 cooling show a large increase in the product of allowable current and/or half-length L. In LN_2 a turn with L = 4 cm could carry only about 60 A rms. In LH_2, for the same length, a current of 195 A rms is possible. Or for the same current (60 A rms) a half-length of 13.5 cm is allowed. The advantage at LH_2 temperature can be split both ways, as shown by the result for 80 A rms in a turn with L = 10 cm. Comparing the limiting cases at the two temperatures shows that the product of J^*L increases by a factor of about 3.5 in going from LN_2 to LH_2. It may be further noted that, at least for the range of current and length we have explored, in LH_2 the limiting phenomenon is usually heat conduction, rather than a failure of nucleate boiling. In LN_2 for our investigated cases, both conduction and boiling approached their limits roughly together.

CONCLUDING REMARKS

We have shown that coils in LN_2, configured to reject heat by nucleate boiling only on the exposed ends of the turns, can carry 10 times the steady current typical at room temperature. A subsection of a motor utilizing such coils produced a specific power comparable to the best we are aware of. Although verification of completely steady state operation remains to be shown, the high performance was achieved at current levels that have been shown to be stable at steady state in free pool boiling coil tests. A simple thermal analysis was shown to approximately predict the coil performance. That analysis predicts much higher performance if LH_2 is used as the coolant.

APPENDIX A. TRANSPORT PROPERTY MODELS AND COOLING MODELS

Copper Resistivity

We make a linear approximation to the resistivity of Cu for the region above LN_2 and a quadratic approximation above LH_2 temperature (resistivity in ohm-m):.

$$\rho_{LN2} = (0.00703 * T - 0.3432)*10^{-8} \quad (77K <= T <= 300K) \tag{A1}$$

$$\rho_{LH2} = (0.017+0.0002*(T-20.3)+0.00005*(T-20.3)^2)*10^{-8} \quad (20K<=T<= \sim 100K) \tag{A2}$$

The LH_2 fit is based on a specified residual resistivity ratio (room temperature resistivity divided by the low temperature limit of resistivity) of 100 and the "ideal resistivity" of copper from White & Woods (1959) as reported in [13]. Equations (10) and (11) are plotted in FIGURE 7 along with the ideal resistivity from [13] and the sum of the ideal resistivity and a residual resistivity yielding a residual resistivity ratio of 100.

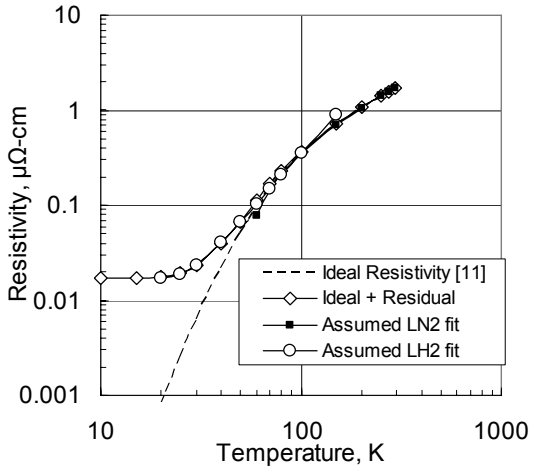

FIGURE 7. Resistivity models for the two temperature ranges compared with an idealized copper resistivity with a residual resistance ratio of 100.

Copper Thermal Conductivity

The thermal conductivity of commercial wire grade copper was taken as 5.5 W/cm-K for the LN_2 temperature range and 12 W/cm-K for the LH_2 temperature range. The latter is slightly lower than that indicated by "Curve P.R.R. – ETP Cu" in FIGURE 43(b) of [14].

LN_2 and LH_2 Nucleate Pool Boiling

Nucleate pool boiling is modeled based on the data from [15] as reported in [16]. The surface heat fluxes Qdot from those references can be fit with the following power laws and are shown in FIGURE 8:

$$\text{Qdot } (LN_2) = 0.0486 * (T - 77)^{2.4} \text{ (W/cm}^2\text{)} \quad \text{(A3)}$$

$$\text{Qdot } (LH_2) = 0.496 * (T - 20.3)^{2.52} \text{ (W/cm}^2\text{)} \quad \text{(A4)}$$

It may be noted that the maximum heat flux in nucleate pool boiling in LH_2 is only half that in LN_2. However, for any given heat flux, the superheat of the surface above the bulk liquid temperature is only about a third as much in LH_2 as in LN_2.

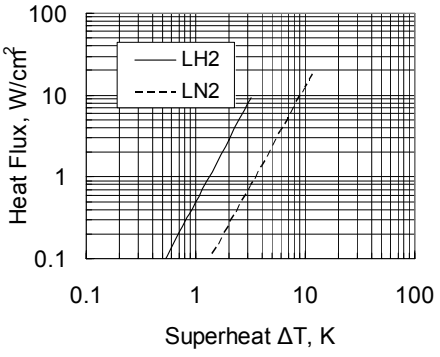

FIGURE 8. Pool nucleate boiling heat flux for LN_2 and LH_2.

REFERENCES

1. Taylor, Clyde E. and Post, Richard F., "Cryogenic Coils," *High Magnetic Fields*, proceedings of the International Conference on High Magnetic Fields, held at MIT, Cambridge, MA, Nov 1-4, 1961, ed. H. Kolm, B. Lax, F. Bitter and R. Mills, MIT Press & John Wiley & Sons, New York, 1962 pp. 101-108.
2. Laquer, Henry L., "The Cryogenic Magnet Program at Los Alamos," ibid, pp 156-165.
3. Purcell, "An Aluminum Magnet Cooled with Liquid Hydrogen," ibid, pp 166-169.
4. Laurence, James C., Brown, Gerald V., Geist, Jacob and Zeitz, Kenneth, "A Large Liquid-Neon-Cooled-Electromagnet," ibid, pp. 170-179.
5. Brown, Gerald V. and Coles, Willard D., "High-Field Liquid-Neon-Cooled Electromagnets," in *Advances in Cryogenic Engineering*, proceedings of the Cryogenic Engineering Conference, Houston, TX, Aug. 23–25, 1965.
6. Oberly, C.E. and Ho, J.C., "The Origin and Future of Composite Aluminum Conductors," *IEEE Transactions on Magnetics*, Vol. 27, No. 1, January 1991. ieeexplore.ieee.org/iel1/20/3154/00101076.pdf?arnumber=101076
7. Shively, Russell, "Submerged Cryogenic Motor Materials Development," *IEEE Electrical Insulation Magazine*, May/June 2003, Vol. 19, No.3, pp. 7-11.
8. Oberly, Charles, "Lightweight Superconducting Generators for Mobile Military Platforms," Proceedings of the PES Meeting 2006, Montreal, Quebec.
9. Brewer, G. Daniel, *Hydrogen Aircraft Technology*, CRC Press, Inc., 1991.
10. Brown, Gerald V., Kascak, Albert F., Ebihara, Ben, Johnson, Dexter, Choi, Benjamin, Siebert, Mark and Buccieri, Carl, "NASA Glenn Research Center Program in High Power Density Motors for Aeropropulsion," NASA/TM—2005-213800, 2005, http://gltrs.grc.nasa.gov/reports/2005/TM-2005-213800.pdf.
11. Radun, Arthur V., "High-Power Density Switched Reluctance Motor Drive for Aerospace Applications," *IEEE Transactions on Industry Applications*, vol. 28, no. 1, Jan./Feb. 1992.
12. Oberly, Charles, "Lightweight Superconducting Generators for Mobile Military Platforms," Proceedings of the PES Meeting 2006, Montreal, Quebec.
13. Hall, L.A., "Survey of Electrical Resistivity Measurements on 16 Pure Metals In the Temperature Range 0 to 273 °K," NBS Technical Note 365, National Bureau of Standards, U.S. Department of Commerce, 1968.
14. Childs, Gregg E., Ericks, Lewis J. and Powell, Robert L., *Thermal Conductivity of Solids at Room Temperature and Below—a Review and Compilation of the Literature*, National Bureau of Standards Monograph 131, 1973.
15. Brentari, E.G. and Smith, R.V., "Nucleate and Film Pool Boiling Design Correlations for O_2, N_2, H_2, and He," *International Advances in Cryogenic Engineering Proceedings*, 1964 Conference, p. 327 for LN_2, p. 331 for LH_2, Plenum Press, 1965.
16. Flynn, Thomas M., *Cryogenic Engineering*, Second Edition, Marcel Dekker, 2005, p. 65—LN_2, p. 66—LH_2.